AGU PUBLICATIONS

JGR

Journal of Geophysical Research: Atmospheres

RESEARCH ARTICLE
10.1002/2016JD025012

Special Section:
Energetic Electron Loss and its Impacts on the Atmosphere

Sensitivity of simulated mesospheric transport of nitrogen oxides to parameterized gravity waves

Katharina Meraner[1], Hauke Schmidt[1], Elisa Manzini[1], Bernd Funke[2], and Angela Gardini[2]

[1] Max Planck Institute for Meteorology, Hamburg, Germany, [2] Instituto de Astrofísica de Andalucía, CSIC, Granada, Spain

Key Points:
- Sensitivity of simulated polar winter NOx transport to parameterized gravity wave sources is explored
- Weakening of gravity wave sources enhances mesospheric transport
- Altitude at which momentum is deposited controls the downward transport of NOx

Correspondence to:
K. Meraner,
katharina.meraner@mpimet.mpg.de

Citation:
Meraner, K., H. Schmidt, E. Manzini, B. Funke, and A. Gardini (2016), Sensitivity of simulated mesospheric transport of nitrogen oxides to parameterized gravity waves, *J. Geophys. Res. Atmos.*, *121*, 12,045–12,061, doi:10.1002/2016JD025012.

Received 28 FEB 2016
Accepted 4 OCT 2016
Accepted article online 8 OCT 2016
Published online 25 OCT 2016

Abstract Gravity waves strongly influence the circulation and transport processes in the middle atmosphere. We analyze the sensitivity of the simulated mesospheric transport of nitrogen oxides (NO_x) to differences in a parameterization of nonorographic gravity waves. After particularly strong sudden stratospheric warming (SSW) events as in January 2009, satellite instruments measured a strong mesospheric descent of NO_x. However, this downward transport is in general underestimated in models covering this altitude range. We use simulations of the atmospheric general circulation and chemistry model HAMMONIA (Hamburg Model of Neutral and Ionized Atmosphere) to discuss both differences in a homogeneous background gravity wave source and a source related to frontal activity. The results show that the transport of NO_x is highly sensitive to such differences. With a stronger gravity wave source, less NO_x is transported after the SSW to the mesosphere and the elevated stratopause descends more rapidly to its climatological altitude. We observe the opposite by weakening the gravity wave sources yielding a better agreement with the observations. The amount of the transported NO_x is controlled by the altitude at which momentum is deposited in the atmosphere. The higher the altitude where the momentum is deposited in the upper mesosphere, the stronger is the descent of NO_x. A small wave amplitude favors the transition to turbulence at a higher altitude due to the exponential increase of the amplitude with height.

1. Introduction

The large-scale circulation of the middle atmosphere is strongly influenced by the momentum deposition from gravity waves that propagate upward from tropospheric sources. The momentum deposition is the main driver for the mesospheric mean meridional circulation with upwelling in the summer and downwelling in the winter hemisphere [*Holton et al.*, 1995; *Haynes et al.*, 1991; *Alexander et al.*, 2010]. The latter enables the transport of tracers from the mesopause to the stratosphere and is therefore a key process for the potential influence of thermospheric nitrogen oxides (NO_x) produced by energetic particle precipitation on stratospheric ozone and subsequently stratospheric circulation and surface climate [*Randall et al.*, 2007; *Rozanov et al.*, 2005; *Baumgaertner et al.*, 2011; *Seppälä et al.*, 2009].

Recent satellite observations measured an enhancement of the downward transport of NO_x after sudden stratospheric warming (SSW) events. *Randall et al.* [2009] showed that the NO_x amount which descended from the thermosphere to the stratosphere after the SSW in 2009 was 50 times higher than during undisturbed conditions. However, the assessment of mesospheric descent of NO_x and CO after the 2009 SSW in observations and general circulation models covering this altitude range, currently being conducted within Stratospheric Processes and their Role in Climate's SOLARIS-HEPPA project, indicates that the modeled descent is generally too weak. This underestimation is speculated to be due to deficiencies in the representation of either advective or diffusive mesospheric transport [*Smith et al.*, 2011; *Holt et al.*, 2013], which are both largely caused by dissipating gravity waves. In a study with the Hamburg Model of Neutral and Ionized Atmosphere (HAMMONIA) which is also used here, *Meraner and Schmidt* [2016] showed that after a SSW event, NO_x is predominantly transported by advection from the polar thermosphere downward. The contribution of molecular diffusion is limited to the thermosphere, and eddy diffusion only contributed marginally. Changes of the circulation could, hence, have a strong impact on the descent of NO_x.

In this study, we analyze the sensitivity of the simulated transport of NO_x to differences in the gravity wave parameterization in the general circulation and chemistry model HAMMONIA. Due to the small horizontal wavelength of gravity waves, their effects on the circulation need to be parameterized in most general circulation models of the middle atmosphere.

McLandress et al. [2013] stated that after a SSW, advection is strongly forced by nonorographic gravity waves. They carried out simulations with the Canadian Middle Atmosphere Model with sources of either the orographic or the nonorographic gravity waves switched off for the dynamically perturbed northern winters of 2006 and 2009. They found that without orographic gravity waves, the upper mesospheric downwelling under undisturbed conditions is twice as strong as in the control run. Furthermore, the relative importance of the two types of gravity waves depends on the time with respect to the central date of the SSW. After the SSW when the westerlies are too weak to allow much vertical propagation of the orographic gravity waves to the mesosphere, the nonorographic gravity waves drive the circulation and thereby the descent of tracers (e.g., CO and NO_x) from the thermosphere. Moreover, *Siskind et al.* [2015] showed that models have deficits in simulating the nonorographic gravity wave forcing and suggested that a weak mesospheric descent is caused by an underestimation of the nonorographic gravity wave drag.

However, due to the small spatial scale of large parts of the gravity wave spectrum, constraining gravity wave drag from global satellite observation remains a challenge [e.g., *Geller et al.*, 2013; *Alexander*, 2015]. The resulting uncertainty makes it necessary to tune gravity wave parameterizations in general circulation models (GCMs) and in particular the gravity wave sources to reproduce available macroscale observations. Common constraints are to simulate realistic climatological zonal winds or a realistic quasi-biennial oscillation [e.g., *Richter et al.*, 2010; *Scaife et al.*, 2000]. In a similar sense, *McLandress et al.* [2013] suggested that also observations of the downward transport of NO_x data may be used to provide additional constraints for gravity wave sources in numerical models.

Following *McLandress et al.* [2013] this paper determines the impact of the nonorographic gravity wave parameterization on simulations of the NO_x transport. We use simulations with the general circulation and chemistry model HAMMONIA, in which we either modify the homogeneous background source of gravity waves or a source related to tropospheric fronts. The simulations are evaluated against observational data taken by Michelson Interferometer for Passive Atmospheric Sounding (MIPAS)/Envisat. We concentrate on the winter 2009, because the major SSW event in January 2009 was the strongest and most prolonged on record [*Manney et al.*, 2009]. Additionally, after the final breakdown of the recent stratopause the new stratopause reformed in early February near 80 km. This reformation of the new stratopause at an anomalously high level is called an elevated stratopause event and is an indicator of enhanced descent in the mesosphere and lower thermosphere [*Siskind et al.*, 2007].

Our study aims at a better understanding of the role of gravity waves for the downward transport of NO_x during the northern hemisphere winter in relation to SSWs and thereby to allow for a better estimation of potential geomagnetic effects on climate. [*Seppälä et al.*, 2009; *Baumgaertner et al.*, 2011]. Furthermore, we discuss to what extent the observed mesospheric downward transport in nudged simulations may be used to further constrain gravity wave sources as suggested by *McLandress et al.* [2013]. Our study extends the sensitivity analysis by *Charron and Manzini* [2002], who used a model with a top of 0.1 hPa, while HAMMONIA treats the dynamics up to 10^{-7} hPa. Moreover, our study sheds light on the importance of anomalous gravity wave filtering for the disturbed mesospheric dynamics observed during SSWs, e.g., the cooling of the lower mesosphere [e.g., *Siskind et al.*, 2005; *Limpasuvan et al.*, 2012] or the occasional occurrence of an elevated stratopause [e.g., *Tomikawa et al.*, 2012]. Additionally, the possible interaction between resolved waves and gravity waves as reported, e.g., by *Sigmond and Shepherd* [2014] and *Chandran et al.* [2013], is discussed. Especially, after a SSW the effect of nonorographic gravity waves is amplified by resolved waves [*Limpasuvan et al.*, 2016]. *Manzini and McFarlane* [1998] reported compensation of resolved and gravity waves in the lower mesosphere in the northern hemisphere.

This paper is organized in the following way: section 2 describes the model setup and the observations. Section 3 shows the impact of the background source and the frontal source on the transport and explains the importance of the altitude of momentum deposition for the strength of the transport. Finally, section 4 summarizes and discusses the main outcomes as well as the limitations of the study.

2. Model and Observational Data

2.1. HAMMONIA: The Hamburg Model of the Neutral and Ionized Atmosphere

HAMMONIA is an upward extension of ECHAM5 GCM [*Roeckner et al.*, 2006] coupled to the MOZART3 chemistry model [*Kinnison et al.*, 2007]. Atmospheric dynamics, radiation, and chemistry are treated interactively from the surface to the thermosphere (approximately 250 km altitude). A detailed description of the model

is given in *Schmidt et al.* [2006]. To include the electron impact on NO production, we enhanced the model to incorporate the ion chemistry of the ionospheric *E* and *F* region as described in *Kieser* [2011] and *Meraner and Schmidt* [2016]. *Siskind et al.* [2015] stated that an additional source of NO from high energetic particle precipitation is not needed. In this study, HAMMONIA is run with a triangular truncation at wave number 63 (T63), corresponding to a resolution of about 1.9° in latitude and longitude, and with 119 vertical layers. The vertical resolution varies between 800 m in the upper troposphere and 3 km in the lower thermosphere. Sea surface temperature and sea ice cover are taken from the Atmospheric Model Intercomparison Project 2 climatology. Present-day conditions of greenhouse gas concentrations are used. EUV-related thermospheric NO production corresponding to solar minimum is parameterized as function of the $F_{10.7}$ solar flux ranging from 64 to 74 10^{-22} Wm^{-2} Hz^{-1} for the period under investigation. Total and spectral solar irradiance are as well specified for the 2009 solar minimum. The particle-induced ion pair production rates are provided by the Atmospheric Ionization Module Osnabrück (AIMOS version 1.6) [*Wissing and Kallenrode*, 2009].

Two parameterizations are used to describe gravity wave processes. Orographic waves and surface blocking are parameterized according to *Lott and Miller* [1997], while nonorographic gravity waves are parameterized according to the Doppler spread theory from *Hines* [1997a, 1997b]. As stated above, we concentrate on studying the sensitivity of the tracer transport to nonorographic gravity waves and, hence, the parameterization of the orographic gravity waves remains unchanged. The Hines parameterization considers a broadband and continuous spectrum arising from a variety of forcing mechanisms (e.g., shear instability and convective activity). It is assumed that all sources are located in the troposphere and that the generated gravity waves exclusively propagate vertically. In this study, we use a geographically uniform isotropic gravity wave source spectrum with a constant root-mean-square (RMS) wave wind speed launched at 830 hPa (σ). The RMS wind speed describes the strength of the gravity wave source (i.e., the amplitude of the waves). The default value is 0.8 m/s.

While the homogeneous background source of gravity waves is independent of the actual simulated meteorology, HAMMONIA additionally offers the option to include tropospheric fronts as a gravity wave source following *Charron and Manzini* [2002]. The parameterization assumes that frontogenesis occurs when a strong deformation of the wind field increases the horizontal temperature gradient. If the threshold of 0.1 K^2 $(100\ km)^{-2}$ h^{-2} is reached, a gravity wave spectrum is emitted but with an RMS wave wind speed of 2 m/s instead of 0.8 m/s. Hence, at the location of fronts the homogeneous source is replaced by the frontal source of *Charron and Manzini* [2002] and no gravity waves are emitted from the background. The homogeneous source with an RMS wind speed of 0.8 m/s is only used in at grid points where no frontal source is used. Gravity waves excited by fronts are emitted in the two cross-front directions (perpendicular to the tropospheric winds associated with the fronts).

As gravity waves propagate upward, the wave action is conserved until the gravity wave spectrum as a whole becomes unstable and waves at high vertical waves at high vertical wave number break down into turbulence. The transition to turbulence is parameterized according to *Hines* [1997a, 1997b] to occur at a specific wave number, called the cutoff wave number. It is assumed that waves with a wave number larger than the cutoff wave number are removed from the spectrum and the momentum they carried is deposited into the background flow. This, in turn, influences the middle atmospheric dynamics and thereby the advection, which dominates the transport of tracers below the mesopause [*Meraner and Schmidt*, 2016].

We analyze the sensitivity of the tracer transport to two modifications of gravity sources: (1) switching on/off the emission of gravity waves from fronts and (2) varying the strength of the homogeneous background source. We carried out four experiments running from January to April 2009, which are summarized in Table 1. Compared to the control simulation, two experiments consider a strengthening of gravity wave sources (i.e., an increase of the wave amplitude), either by switching on the emission of gravity waves from fronts (front on) or by increasing σ from 0.8 to 1.0 m/s (strong background). In the fourth experiment gravity wave sources are weakened via a reduction of σ to 0.6 m/s (weak background). Note that by switching on the emission of gravity waves from fronts, not only the wave amplitude (i.e., the RMS wave wind speed) but also the orientation of the phase speed are modified. In earlier studies of HAMMONIA either the "front on" configuration [e.g., *Funke et al.*, 2011] or the "strong background" configuration [e.g., *Pedatella et al.*, 2014] is used.

In all four simulations, surface pressure, temperature, divergence, and vorticity are nudged (i.e., relaxed) from 850 hPa to 1 hPa with an upper and lower transition zone. The nudging data are 6-hourly values of the

Table 1. List of Nudged Experiments with Gravity Waves From Fronts (lfront) Either Switched on (True) or Switched Off (False) and Different RMS Wave Wind Speeds (σ) of the Background Source[a]

Experiment	lfront	σ (m/s)
Control	False	0.8
Front on	True	0.8
Weak background	False	0.6
Strong background	False	1.0

[a]Note that the frontal source is launched with a RMS wave wind speed of 2 m/s.

European Centre for Medium-Range Weather Forecasts Interim Re-Analysis [*Dee et al.*, 2011]. The nudging assures that the model captures the tropospheric and stratospheric dynamics as observed during the winter 2009, including the major SSW event in January 2009. As long as the critical-level filtering of gravity waves in the troposphere and stratosphere is captured, the upper atmosphere is strongly constrained through the nudging without the need of explicitly nudging the mesospheric temperature [*Ren et al.*, 2011]. Temperature and NO_x of these experiments are compared to MIPAS (Michelson Interferometer for Passive Atmospheric Sounding), and thereby, averaging kernel filtering is applied. For temperature, the simulations are filtered based on the average diagonal element of the averaging kernel matrix with a threshold of 0.03. For NO_x, latitudinal bins are rejected when the average of the averaging kernel diagonal element is larger than 0.03.

In addition to the nudged simulations, we performed two free-running simulations lasting 49 years. To make them comparable to the nudged simulations, we used the same boundary conditions as for the nudged simulations (fixed SST, greenhouse gases, and solar and energetic forcing from June 2008 to May 2009). The only difference between the nudged and the free-running simulations, hence, is the nudging. To explore the sensitivity of the transport of NO_x to extreme cases, two experiments were carried out, which correspond to the "front on" and "weak background" experiments. We concentrate our analysis on the high latitudes. Therefore, all following figures show polar cap averages (60°N–90°N) unless otherwise stated.

2.2. MIPAS: Michelson Interferometer for Passive Atmospheric Sounding

MIPAS is a midinfrared Fourier transform limb emission spectrometer [*Fischer et al.*, 2008] on board of the European Environmental Satellite (Envisat). The instrument measured atmospheric trace species from March 2002 to April 2012. The retrieval of the gas and temperature profiles has been performed using the level 2 processor developed by the Institute of Meteorology and Climate Research of the Karlsruhe Institute of Technology and the Instituto de Astrofísica de Andalucía. Here we use temperature (V5_220 and V5_521) [*García-Comas et al.*, 2014] and NO_x (V4_220 and V4_501) [*Funke et al.*, 2005] data from January to April 2009. The data are derived from the nominal below 0.02 hPa and from the middle and upper atmosphere observation mode above 0.02 hPa. The nominal observational mode measured regularly on an almost daily basis and covered an altitude range from 7 to 70 km. MIPAS measured in the middle and upper atmosphere mode only between 1 to 12 days per month and covered an altitude range of 20–102 km. We interpolate 2-hourly gridded HAMMONIA data to the actual measurement times and locations of MIPAS.

MIPAS temperature and NO_x agree very well with other satellite measurements (e.g., the Atmospheric Chemistry Experiment Fourier Transform Spectrometer observation) and ground-based observations [*Bender et al.*, 2015; *García-Comas et al.*, 2014]. *Meraner and Schmidt* [2016] showed that the MIPAS vertical NO profile is reasonably reproduced by HAMMONIA.

3. Results

3.1. Sensitivity of Temperature and NO_x Transport to Gravity Wave Sources in Nudged Simulations

In the following, we analyze the changes in the temperature and transport of NO_x due to variations in the gravity wave parameterization. We discuss differences in the homogeneous background source and in the source related to frontal activity. All HAMMONIA experiments are compared to MIPAS observations. First, we explore the changes in the temperature and in NO_x due to switching on/off the emission of gravity waves excited by fronts. Note that at the locations where frontal gravity waves are excited no additional background source is considered.

Figures 1a, 1c, and 1d show the temperature for January to April 2009 including the major SSW event in late January. On 24 January 2009, a reversal of the northern polar vortex westerlies occurred due to anomalous wave-2 activity in the upper troposphere [*Manney et al.*, 2009]. Subsequently, the stratopause warmed,

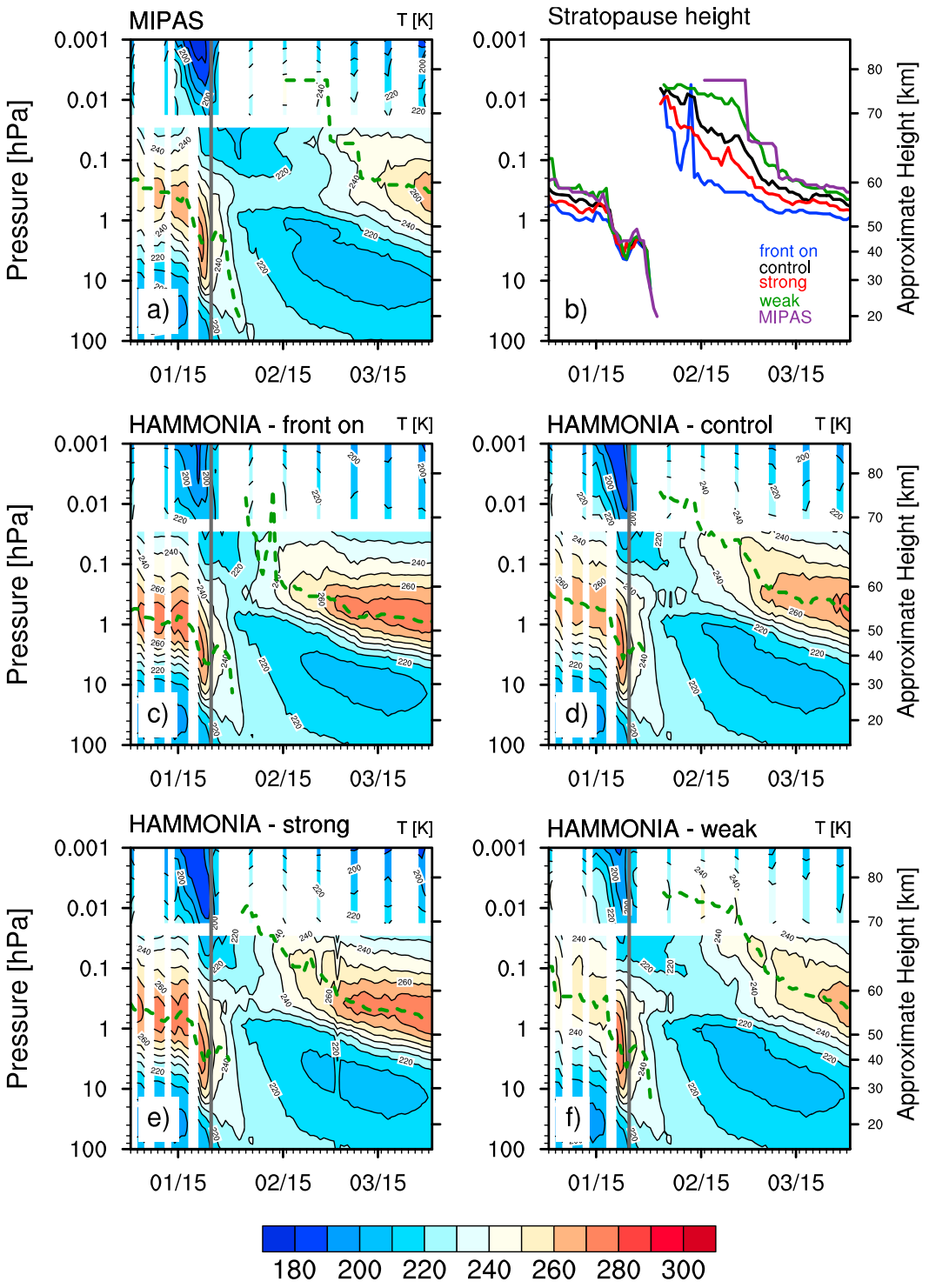

Figure 1. Temperature averaged over the polar cap (60°N–90°N) for January to April 2009 in (a) MIPAS and four HAMMONIA simulations: (c) with gravity waves induced by fronts, (d) control experiment (σ = 0.8 m/s), (e) with a strong background source (σ = 1.0 m/s), (f) with a weak background source (σ = 0.6 m/s). For Figures 1d–1f gravity waves from fronts are switched off. The contour interval is 10 K. (b) The height of the stratopause for MIPAS and all four HAMMONIA experiments. The gray solid line corresponds to the central date of the SSW (24 January 2009). The height of the stratopause of MIPAS (Figure 1a) and the individual experiments (Figures 1c–1f) is marked by the green dashed line.

dropped below 30 km and finally broke down in late January. At the same time, the mesosphere cooled. In mid-February the elevated stratopause reformed at an anomalously high altitude (near 80 km) and descended thereafter to its climatological altitude.

The stratopause is determined as the first local temperature maximum above the tropopause and is located near 0.3 hPa during undisturbed conditions (see Figure 1a). Compared to MIPAS, the stratopause under undisturbed conditions (early January) is about 11 K too warm in the experiment front on. The control experiment produces a colder stratopause that agrees better with MIPAS (only 6 K too warm). The warming and displacement of the stratopause to a lower altitude after 24 January is well reproduced in both HAMMONIA simulations. Note that the model is nudged up to 1 hPa to the ERA-Interim reanalysis data. Hence, the HAMMONIA experiments only slightly differ below 1 hPa and are similar to the MIPAS observations. Simultaneously with the warming of the stratosphere, the mesosphere cooled. However, the cooling is too weak in the front on experiment (about 20 K too warm compared to MIPAS). The reformation of the elevated stratopause and its descent happen too quickly in HAMMONIA, which is common in models covering this altitude range [*Pedatella et al.*, 2014]. However, in the control experiment the new stratopause stays longer at a higher altitude and reaches its approximate climatological altitude later than for the experiment with gravity waves emitted from fronts (see Figure 1b).

Figures 2a–2c shows a comparison of the NO_x mixing ratio observed by MIPAS to those in the two HAMMONIA experiments, with and without gravity waves excited from fronts. Prior to the SSW, both model simulations show similar NO_x concentrations in the stratosphere and mesosphere. The SSW is characterized by the decrease of NO_x on 24 January 2009, which is caused by enhanced lateral mixing following the split of the polar vortex [*Salmi et al.*, 2011]. Qualitatively, the decrease in NO_x is reproduced in both HAMMONIA simulations, however, weaker than in MIPAS. This deficiency is caused by a too weak horizontal NO_x gradient in HAMMONIA (not shown).

The reformation of the new stratopause led to a strong descent of NO_x and to a development of a tongue-like structure (see Figure 2a). High NO_x amounts were transported to the mesosphere leading to 4 times higher values of NO_x concentrations at 0.1 hPa after the SSW than before the SSW. In early March the NO_x concentrations decreased and dropped even below the pre-SSW level above 0.1 hPa. Hence, at the end of March the amount of NO_x is more than 2 times higher at 1 hPa than at 0.04 hPa. This enhanced descent is associated with the recovery of the polar vortex [*Randall et al.*, 2009].

Both HAMMONIA experiments (front on and control) show the enhancement of the NO_x concentrations after the SSW and a development of a tongue. However, the tongue is not as pronounced in HAMMONIA as it is in MIPAS. This is especially true for the experiment with gravity waves emitted from fronts (see Figure 2b). For this experiment, the NO_x concentrations decreased already on 16 February, while for the control experiment the tongue is still evident until 4 March. Hence, the descent lasts longer in the control experiment resulting in a better agreement with MIPAS than in the experiment with gravity waves emitted from fronts.

In the following, we explore the changes in temperature and in NO_x due to the background source by varying σ (see Figures 1d–1f and 2c–2e). In those experiments the emission of gravity waves by fronts is switched off. The control experiment corresponds to a wave wind speed of 0.8 m/s. Starting from this default background source, we either weaken the background source ($\sigma = 0.6$ m/s) or strengthen the background source ($\sigma = 1.0$).

Figures 1d-1f shows the temperatures from the three HAMMONIA experiments. The main characteristics of the displacement and the reformation of the elevated stratopause are reproduced in all simulations. However, some differences emerge. Compared to the MIPAS observations (see Figure 1a), the stratopause is under undisturbed conditions about 12 K too warm for a strong background source and about 6 K too cold for a weak background source. The cooling of the mesosphere around the central date of the SSW agrees well for a strong background source with MIPAS. With a weak background source, the mesospheric cooling is too weak. All three simulations show an elevated stratopause in early February. However, the descent of the new stratopause is too fast with a strong background source, while the experiment with a weak background source agrees better with the MIPAS observations. With a strong background source, the new stratopause reaches its climatological altitude on 14 March, while for a weak background source this is delayed for 4 days.

Analyzing again the NO_x concentrations of MIPAS and HAMMONIA, the SSW is characterized by the decrease in NO_x on 24 January (see Figure 2a and 2c–2e). HAMMONIA reproduces the decrease in NO_x but again much

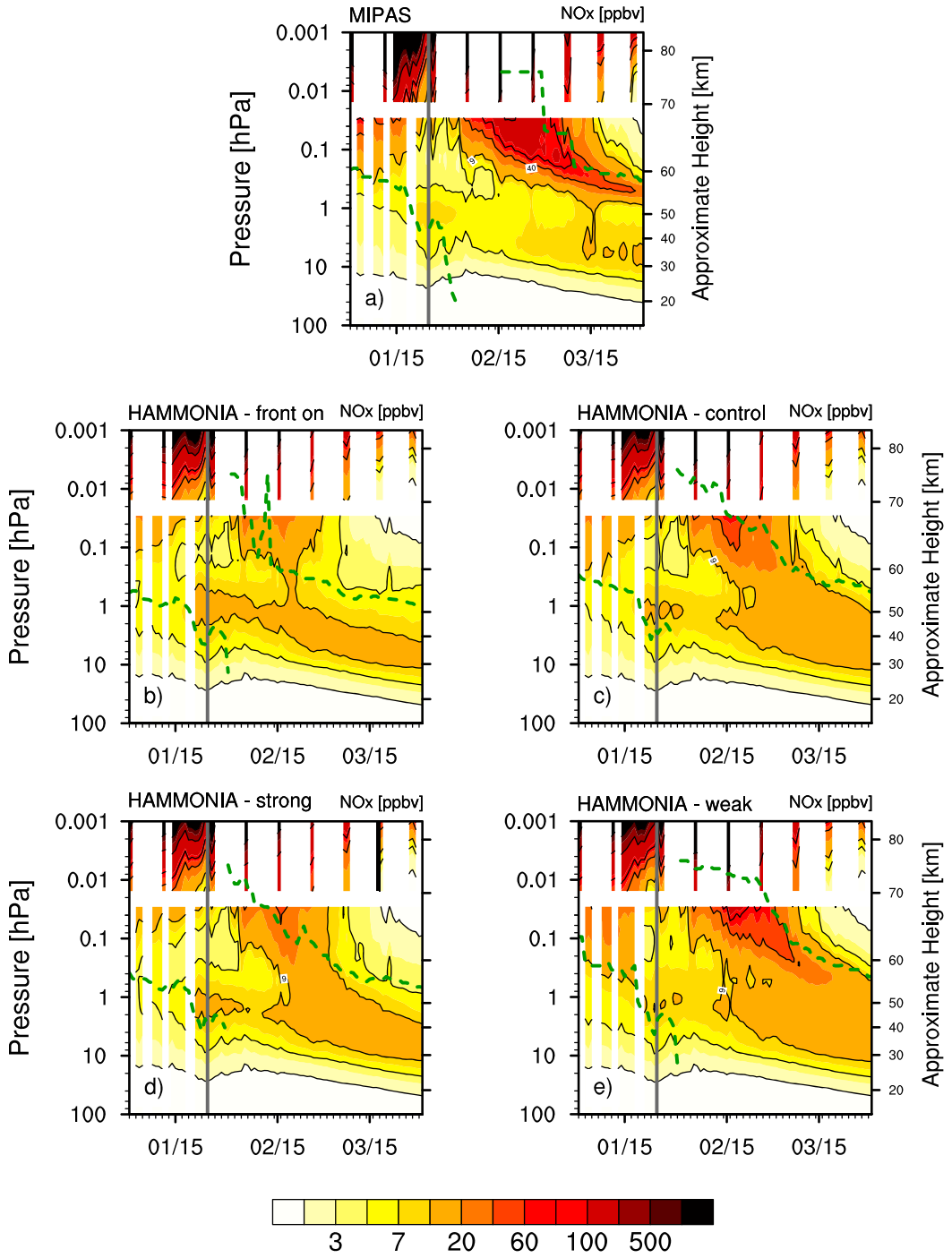

Figure 2. NO_x volume mixing ratio over 60°N–90°N for January to April 2009 in (a) MIPAS and four HAMMONIA simulations: (b) with gravity waves induced by fronts, (c) control experiment (σ = 0.8 m/s), (d) with a strong background source (σ = 1.0 m/s), (e) with a weak background source (σ = 0.6 m/s). For Figures 2c–2e gravity waves from fronts are switched off. The gray solid line corresponds to the central date of the SSW (24 January 2009). The height of the stratopause of MIPAS (Figure 2a) and the individual experiments (Figures 2b to 2e) is marked by the green dashed line.

weaker than MIPAS (see above). In the experiment with a weak background source the NO_x concentrations in early January are increased around 0.04 hPa compared to the control experiment.

Along with the reformation of the new stratopause at an unusually high altitude, high NO_x concentrations are transported downward in all simulations. However, the duration and the actual amount of transported NO_x varies. With a strong background source, less NO_x is transported to 0.04 hPa compared to the default background source (control experiment). Already on 18 February, the NO_x concentrations decrease at 0.04 hPa and the tongue becomes indistinguishable from the background NO_x. This occurs earlier than in the control experiment (24 February). With a weak background source, more NO_x is transported to 0.04 hPa compared to the control experiment. The tongue is more elongated than with a strong background source and becomes only indistinguishable from the background NO_x on 18 March (at 0.4 hPa).

Until now, we have discussed how temperature and NO_x concentrations change due to variations of two gravity wave sources. We either decreased the background source or increased the sources in two different ways: either (a) by allowing the emission of gravity waves from fronts or (b) by strengthening the background source. Compared to the control experiment, both ways of increasing the gravity wave sources show a similar behavior: The undisturbed stratopause is slightly too warm, the elevated stratopause descends too fast to its climatological altitude, and the descent of high NO_x amounts stopped too early. However, some differences emerge, e.g., the tongue in NO_x is more pronounced in the experiment with a strong background than in the experiment with gravity waves emitted from fronts. On the whole, the experiment with a weak background shows the best agreement with MIPAS in terms of temperature and NO_x concentration. In section 3.2 we will link the seen changes in NO_x and temperature to an upward shift of the altitude of the momentum deposition in the upper mesosphere.

3.2. Linking NO_x Transport and Gravity Wave Drag

In this section, we explain the simulated effects on NO_x concentrations by analyzing the resulting residual vertical wind and the wave forcing. Figure 3 shows the changes in vertical wind and temperature caused by increasing the gravity wave sources (due to the frontal or background source) or by decreasing the gravity wave sources. Both strengthening experiments show similar characteristics (see Figures 3a and 3b): The stratopause in early January (i.e., under undisturbed conditions) is too warm. The descent of the elevated stratopause happens too quickly highlighted by the dipole structure from February to April 2009 (also compare to Figures 1b and 1c, and 1e). However, some differences also emerge between Figures 3a and Figure 3b. The stratopause in front on is in March warmer than in the experiment with a strong background source. Along with the relative cooling of the upper mesosphere, the downwelling weakens as can be seen by the vertical vectors. Note that there is no net upward flow between 10 hPa and 0.001 hPa after the SSW but just weakened downward flow. The strongest weakening of the downwelling occurs in both experiments at different time and altitude: at 0.004 hPa on 26 February for the front on experiment and at 0.0008 hPa on 1 February for the strong background experiment. The weakened vertical wind explains well the lower NO_x concentrations at 0.01 hPa after the SSW in both experiments compared to the control experiment.

If we decrease the gravity wave sources, the above mentioned differences change in sign (see Figure 3c). The stratopause in early January is cooler, and the elevated stratopause remains longer at a higher altitude (see again the dipole structure from February to April 2009 and compare to Figure 1b). Along with the reformation of the new stratopause, the downward vertical wind enhances. The strongest downwelling occurs at a similar time and altitude as the weakened downwelling in the strong background experiment (at 10^{-4} hPa on 6 February). The enhanced downwelling explains well the higher NO_x concentrations after the SSW at 0.01 hPa compared to the control experiment.

In the following, we analyze the influences of the parameterized gravity wave drag and the resolved wave drag on the circulation. The component of gravity wave drag shown describes the forcing of the zonal wind due to momentum deposition of dissipating gravity waves. With decreasing density the drag from momentum deposition increases with height. Thus, the maximum gravity wave drag may not describe the altitude at which most wave breaking is occurring and most momentum is deposited. Note that if we refer to gravity waves, we mean nonorographic gravity waves. The changes in the orographic gravity drag are minimal, likely due to modified propagation conditions caused by changed nonorographic gravity waves.

Figure 4a shows the zonally averaged nonorographic gravity wave drag (per unit mass) for the control experiment. The drag is averaged over 10 February to 12 March 2009. This period is chosen to include the strongest

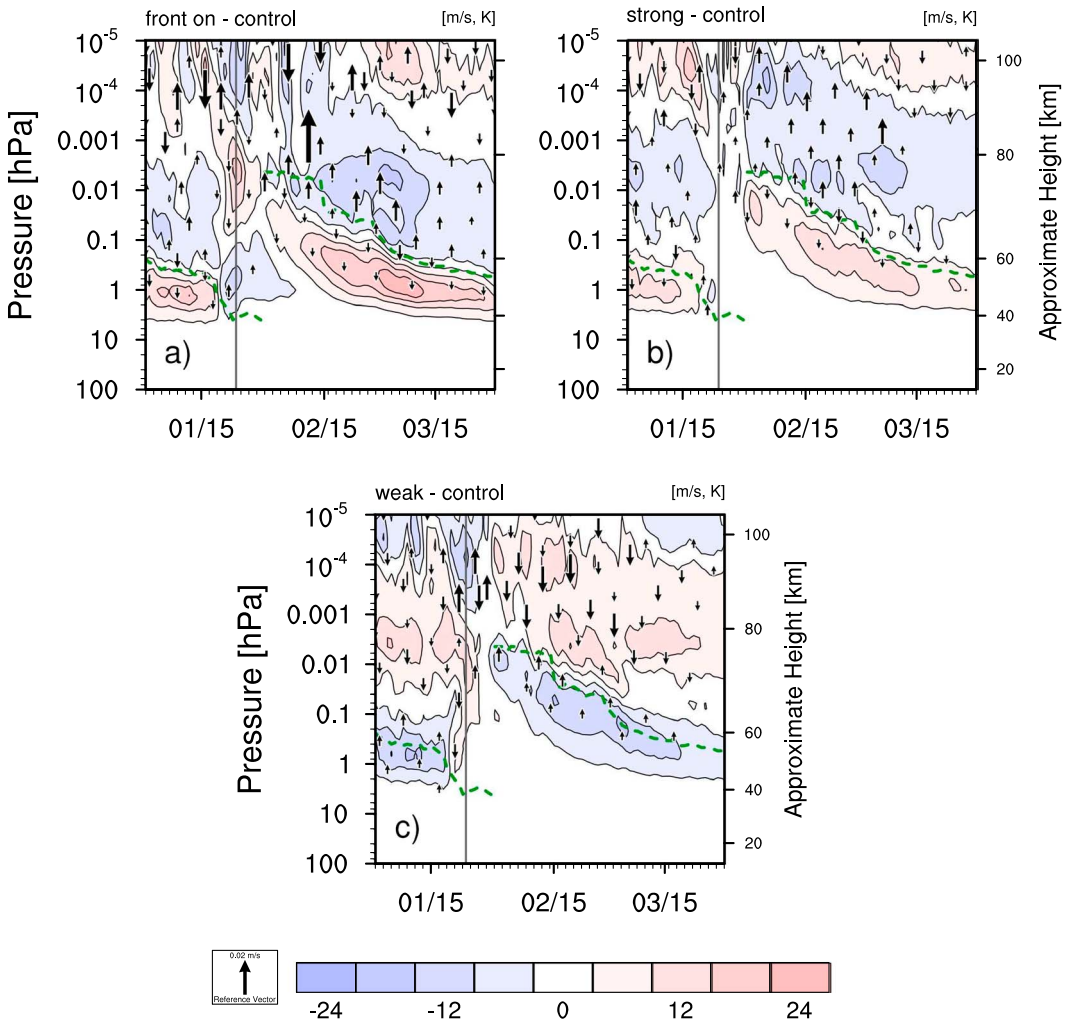

Figure 3. Temperature (colored contours) and residual vertical wind (vectors) differences (K, m/s) for January to April 2009. Anomalies to the control experiment are given for (a) front on, (b) strong background, and (c) weak background. The contour interval is 6 K. The gray solid line corresponds to the central date of the SSW (24 January 2009). The height of the stratopause of the control experiment is marked by the green dashed line. Wind arrows smaller than 0.005 m/s are not shown.

change of the vertical wind in Figure 3. The gravity wave drag is in general negative in the polar winter stratosphere and mesosphere, which means that westward momentum is deposited.

Figures 4b and 4c shows the change in the nonorographic gravity wave drag caused by strengthening the gravity wave sources (due to the frontal or background source). If we increase the gravity wave sources, the altitude of the maximum gravity wave drag drops. However, the actual altitude of the maximum differs between both experiments and is slightly higher for the strong background experiment (0.06 hPa) than for the front on experiment (0.1 hPa). In contrast, if we weaken the background source, the altitude of the momentum deposition is shifted upward compared to the control experiment to 10^{-4} hPa (see Figure 4d). This result agrees well with the enhanced downwelling near 10^{-4} hPa in Figure 3c. The upward shift of the gravity wave drag maximum for a weak background source remains valid also under undisturbed conditions (not shown).

Analogous to the gravity wave forcing, we now analyze the resolved wave forcing as diagnosed by the Eliassen-Palm (EP) flux divergence (see Figure 5). Several studies highlighted the strong interplay of gravity waves and resolved waves, especially after a SSW [e.g., *Limpasuvan et al.*, 2016]. Hence, the transfer of momentum from resolved waves to the mean circulation should be taken into account. Resolved waves exert an easterly force on the zonal mean flow throughout most of the winter middle atmosphere (see Figure 5a). The strongest westward force occurs in the midlatitudes in the upper mesosphere. Above the mesopause a strong

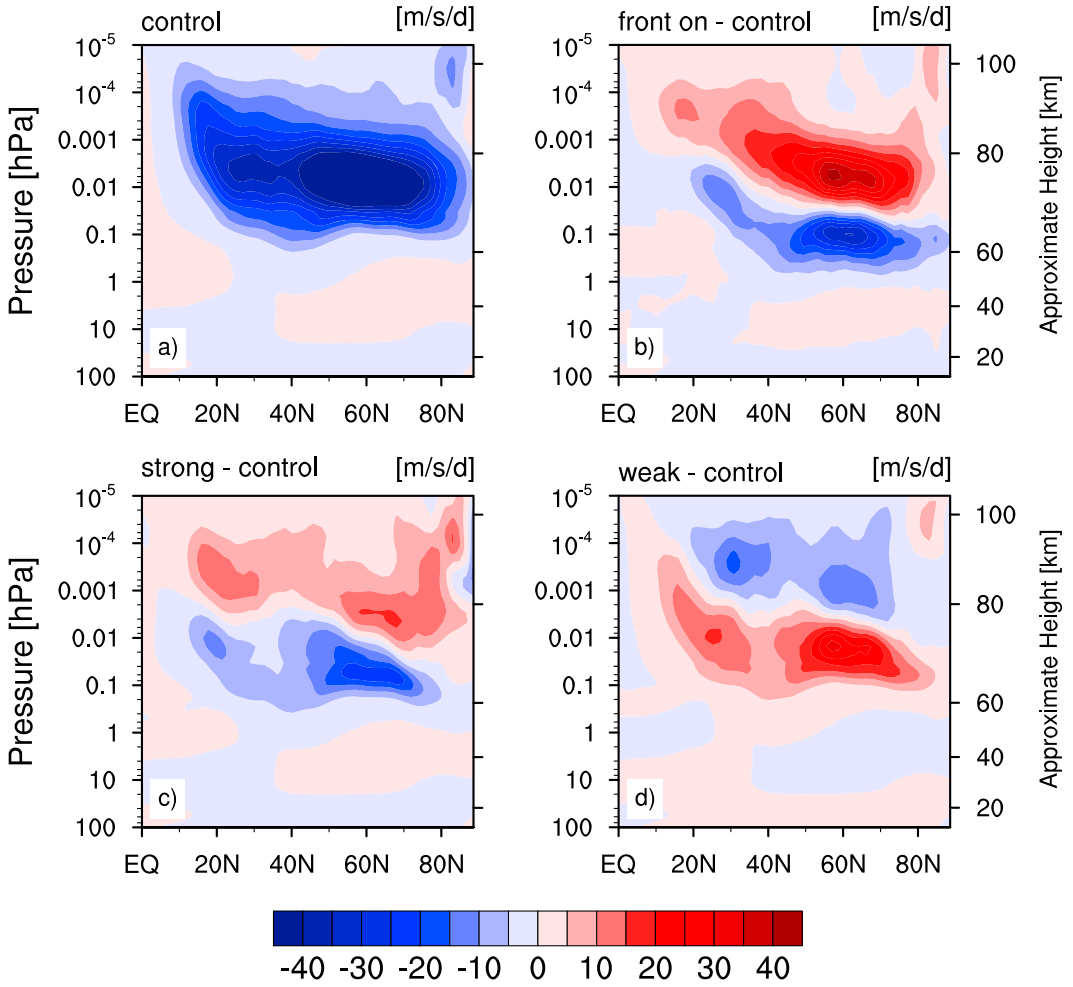

Figure 4. Nonorographic gravity wave drag (m/s/d) for 10 February to 12 March 2009 for (a) control experiment. Differences to the control experiment are given for (b) front on, (c) strong background, and (d) weak background. The contour interval is 5 m/s/d.

deposition of eastward momentum is evident. Figures 5b and c shows the changes in the EP flux divergence by strengthening the gravity wave sources. In those cases, the EP flux divergence is reduced in the high latitudes near 10^{-4} hPa, while at midlatitudes near the mesopause resolved waves tend to reduce the deceleration. In contrast, by weakening the gravity wave sources, the EP-convergence is enhanced above 0.001 hPa (see Figure 5d). This is at a similar height, at which the gravity wave forcing peaks for the weak background case.

Figure 6a shows vertical profiles of the vertical residual wind (w^*). The height of the strongest downwelling is shifted upward to the upper mesosphere for a weaker background source, while for the front on case the vertical wind peaks in the lower mesosphere. Via the downward control principle [*Haynes et al.*, 1991], we split w^* into contributions of different wave forcings (see Figures 6b and 6c). The overall agreement between the directly computed w^* (black line) and the estimate for w^* from the total wave forcing (green line) demonstrates the validity of the downward control estimates. The individual contributions reveal that the downwelling is almost entirely driven by the nonorographic gravity waves, which is consistent with *McLandress et al.* [2013]. If we weaken the gravity background source, the downwelling in the upper mesosphere (up to 10^{-4} hPa) strengthens compared to the control experiment (see Figure 6c). Again, the differences between the control experiment and the "weak background" experiment are mainly due to differences in the nonorographic gravity waves. However, in the upper mesosphere and lower thermosphere resolved waves contribute equally to the strengthening of the vertical wind. Hence, resolved waves amplify the enhanced downwelling caused by gravity waves.

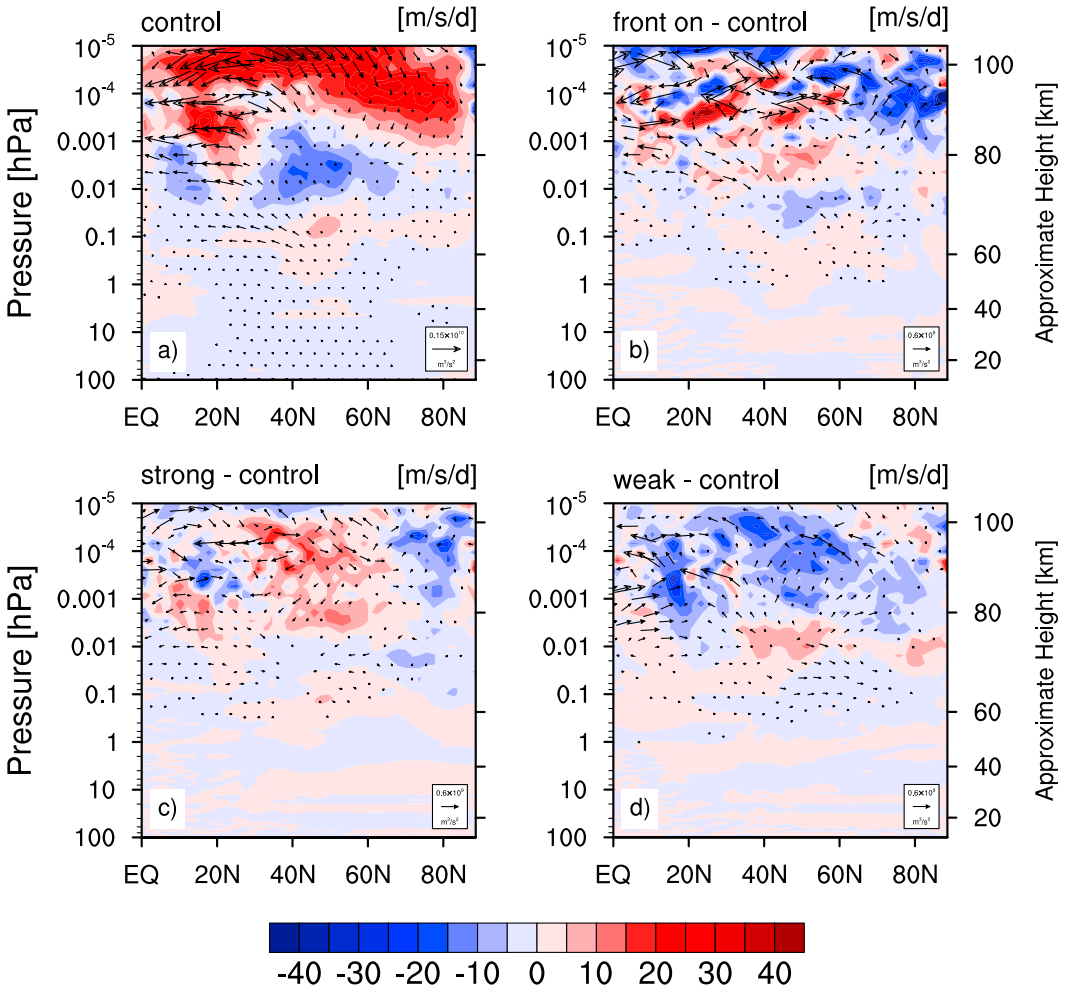

Figure 5. As in Figure 4 but for the resolved wave drag associated with the Eliassen-Palm (EP) flux divergence (contours) (m/s/d). The EP flux (m^3/s^2) scaled by density is depicted by arrows. The contour interval is 5 m/s/d. Arrows smaller than 1.7×10^7 m^3/s^2 are not shown.

We conclude that the altitude at which momentum is deposited by gravity waves in the upper mesosphere has a strong impact on the mesospheric transport. Resolved waves amplify the gravity wave forcing in the recovery phase of a SSW. Even if most momentum is deposited at a much lower altitude (not shown), the momentum deposited in the upper mesosphere is crucial for the mesospheric transport. A deposition of momentum at a higher altitude extends the downwelling branch of the meridional circulation to a higher level (see Figure 6a). Then advection may become the dominant transport process in the lower thermosphere [*Meraner and Schmidt*, 2016], where NO_x is frequently produced by energetic particle precipitation. The downwelling extends upward to the height of the strongest NO_x gradient, and hence, more thermospheric NO_x is transported downward to the lower mesosphere and upper stratosphere. Differences in the gravity wave sources may also influence the contribution of eddy diffusion for the transport to the mesosphere. However, *Meraner and Schmidt* [2016] showed that during a SSW, the downward transport through the mesopause region is dominantly driven by advection. Even with a doubled eddy diffusion coefficient, eddy diffusion has limited impact on the thermospheric transport after a SSW in their experiments. Here changing the gravity wave sources leads to an increase of the eddy diffusion coefficient by only up to a factor of 1.2 (1.7) compared to the control (front on) experiment.

The deposition of horizontal momentum by gravity waves can be modulated by two factors: changes in gravity wave source parameters and changes in the characteristics of the environment in which the waves propagate. Gravity waves break either because the wave amplitude becomes too big and unstable or because the phase speed matches the actual wind speed (critical-level filtering). Without changes in the gravity waves,

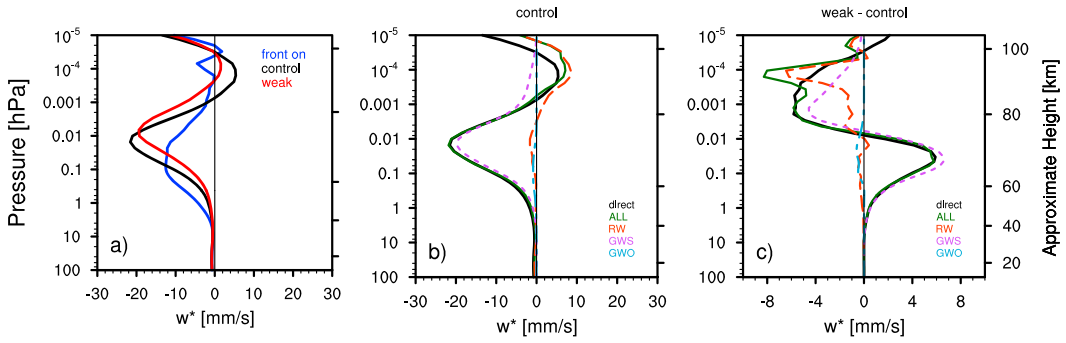

Figure 6. (a) Vertical profile of the residual vertical velocity (w^*) (mm/s) averaged between 60°N and 90°N for 10 February to 12 March 2009 for three experiments: control (black), front on (blue), and weak background (red). (b) Corresponding downward control estimates of the residual vertical velocity in the control experiment computed by using the total wave forcing (green solid line), only the orographic wave drag (cyan dash dotted), only the nonorographic wave drag (purple, short dashed), and only the resolved wave drag (orange long dashed). (c) Differences of the downward control estimates of w^* between the weak background and control experiments are given.

the atmospheric conditions (i.e., the characteristics of the medium) would be very similar for all experiments due to the nudging. However, the gravity wave sources are substantially modified in our experiment by changing the total wind variance (i.e., σ^2).

To understand the changes of the gravity wave drag, we analyze the total wind variance (i.e., the wave amplitude) averaged over the polar cap (60°N–90°N) for three HAMMONIA experiments: control (black), front on (blue), and weak background (red) (see Figure 7). Note that we averaged over the polar cap, thus, locally the total wind variance might be bigger. Substantial filtering by tropospheric winds between the launching height and 500 hPa can explain the relatively small total wind variance at 100 hPa [*Charron and Manzini*, 2002].

The wave amplitude of gravity waves strongly increases from the launching level until 0.1 hPa. This can easily be explained by the fact that without dissipation, the wave amplitude is inversely proportional to the density. The initial total wind variance of gravity waves excited from fronts is greater than the amplitude of gravity waves from the background. Hence, the altitude at which the gravity wave spectrum becomes unstable and breaks into turbulence is lower with gravity waves emitted from fronts than in the control experiment. This conforms to the results of *Charron and Manzini* [2002]. Gravity waves emitted from fronts are parameterized in

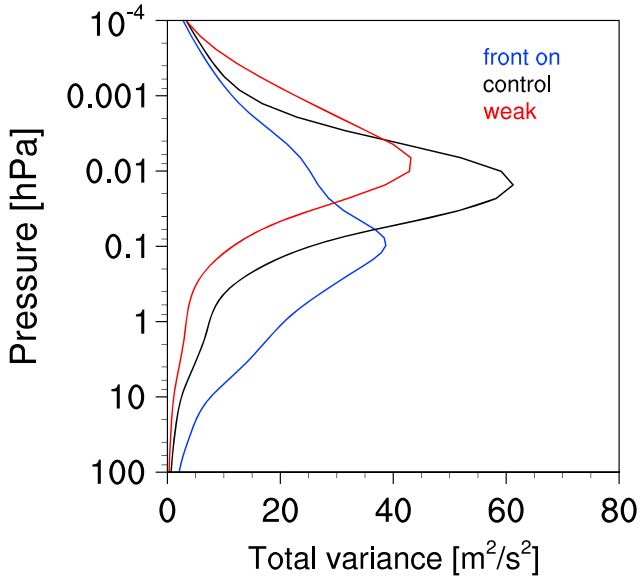

Figure 7. Total gravity wave wind variance ($m^2\ s^{-2}$) on 18 February 2009 averaged between 60°N and 90°N for three experiments: control (black), front on (blue), and weak background (red).

a way that their propagation direction is perpendicular to the tropospheric wind associated with the front. This reduces the critical-level filtering in the troposphere and facilitates the penetration of gravity waves emitted from fronts in the stratosphere [*Charron and Manzini*, 2002]. The total variance of the gravity waves emerging from fronts is small at 0.001 hPa, because most of the transported horizontal momentum is already deposited at a lower altitude.

A similar reasoning applies if we weaken the background source. The total variance at the launching level is reduced compared to the control experiment. Hence, the altitude at which the wave amplitude becomes unstable is higher for a weak background source than in the control experiment. The total variance peaks in this experiment at the highest level of all four experiments. Thus, the small wave amplitude at launching level facilitates the penetration of gravity waves to a higher altitude in the upper mesosphere, where they deposit their momentum, which in turn enhances the mesospheric descent. However, we cannot exclude an impact of the critical-level filtering, because changes in the breaking conditions feed back on the propagation conditions of gravity waves.

We strengthen the gravity wave sources in two ways by either increasing the background or the frontal source. Compared to the control experiment, both cases show a qualitatively similar behavior (e.g., momentum deposition at a lower level in the upper mesosphere). Even if the mean strength of the gravity wave forcing may be the same, it turned out that the momentum flux reaching the middle atmosphere is larger when gravity waves from fronts are present [*Charron and Manzini*, 2002]. This is caused by the reduced critical-level filtering in the troposphere for gravity waves induced by fronts. Additionally, fronts depend on the actual dynamical conditions in the troposphere, and hence, the impact of gravity waves excited by fronts may vary with season and geography.

3.3. Sensitivity of Zonal Wind and NO_x Transport to Gravity Wave Sources in Free-Running Simulations

In the following, we analyze the impact of differences in the gravity wave parameterization in a free-running model. Modifying the gravity wave sources, of course, affects not only the tracer transport but also the mean circulation. However, tropospheric and stratospheric dynamics are constrained to reanalysis data in the nudged simulations. The free-running simulation enables us (1) to estimate the influence of differences in the gravity wave sources on the mean circulation and (2) to assess to which extent the effects on the tracer transport may be specific for the meteorological condition of 2009. We performed two simulations which correspond to the nudged experiments front on and weak background. Those extreme cases are chosen to obtain a large signal to noise ratio. Note that we set up the free-running simulations in a way which facilitates the comparison with the nudged simulations (i.e., we annually repeat boundary conditions valid for the period from June 2008 to May 2009). This setup favors the generation of SSWs, which are in total 61 for the front on and 50 for the weak background experiment.

Figure 8 shows the zonal mean zonal wind of both simulations compared to Modern-Era Retrospective Analysis for Research and Applications (MERRA) [*Rienecker et al.*, 2011] reanalysis data. An average of 37 years (1979–2015) is used for the reanalysis data and of 49 years for the HAMMONIA simulations. The main characteristics (e.g., the subtropical jets) are well reproduced in both simulations. However, some differences emerge between the model simulations and MERRA. For the front on experiment, the stratospheric maximum of the eastward wind in the northern hemisphere is confined between the equator and 60°N, while in the reanalysis data the maximum in the eastward wind extends to the winter pole. Similarly, the westward wind in the southern hemisphere is limited to lower latitudes compared to MERRA. For the weak background experiment, the maximum in the eastward wind expands from the equator to the winter pole and reaches near the pole to a lower altitude than the front on experiment. Both characteristics are consistent with the reanalysis data. The westward wind in the southern hemisphere is tilted toward the summer pole spanning from the equator to the pole, which agrees very well with MERRA. Considering the large number of SSW in the weak background experiments, the magnitude of the eastward wind in the northern hemisphere agrees surprisingly well with the reanalysis data. However, HAMMONIA tends to overestimate the strength of the lower meospheric eastward jet during quiet times (i.e., months without a SSW) (not shown). The large number of SSW weakens the eastward wind bringing it closer to the wind magnitude simulated by MERRA. Overall, the weak background experiment reproduces a more realistic structure of the zonal mean zonal wind and shows a better agreement with MERRA reanalysis data than the front on experiment.

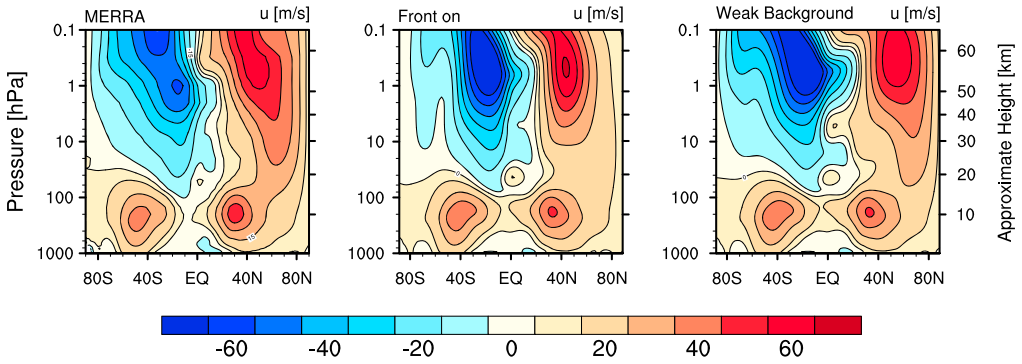

Figure 8. Zonal mean zonal wind averaged over December–February (DJF) for (a) MERRA reanalysis and two free-running simulations (b) with gravity waves from fronts and a medium background (σ = 0.8 m/s) and (c) with a weak background (σ = 0.6 m/s) and no frontal source. The mean over 1979–2015 is used for MERRA and the mean over 49 years for both HAMMONIA simulations. The contour interval is 10 m/s.

Now we evaluate if changes in NO_x transport persist in the free-running simulations (see Figure 9). In the southern hemisphere, differences in NO_x amounts are small between both free-running HAMMONIA simulations. While the northern hemispheric meridional gradient is weak in the front on experiment, the polar NO_x concentrations in the weak background experiment increases by more than 200% near 0.1 hPa compared to the front on experiment. The increase of NO concentration in the mesosphere results from enhanced downwelling near 0.001 hPa (not shown). The higher NO_x concentrations in the mesosphere for a weak background and no frontal source is consistent with the changes in the nudged simulations. This result agrees also with *McLandress et al.* [2013], who found that nonorographic gravity waves cause a strong descent of CO under undisturbed conditions.

Both simulations produce different dynamical responses, e.g., number of SSWs. Thus, one may ask if the simulated effects on the NO_x transport is related to the vertical extension of the downwelling as in the nudged simulations or could be influenced by the higher frequency of major SSWs in the front on experiment. We tested this by comparing the NO_x transport excluding all months in which a major SSW occurs (not shown). The increase in NO_x concentrations occurs similarly for this subset of months, and we conclude that the effects of changed gravity wave sources on the tracer transport are not only specific for the meteorological condition of 2009. Additionally, we have only looked at a subset of climatological changes (i.e., zonal wind and NO_x concentrations), while other aspects may also vary. For example, the winter (summer) mesopause warms (cools) by about 5 K in the weak background experiment compared to the front on experiment (not shown). Compared to the lidar measurements of *Lübken and von Zahn* [1991], the winter (summer) mesopause in

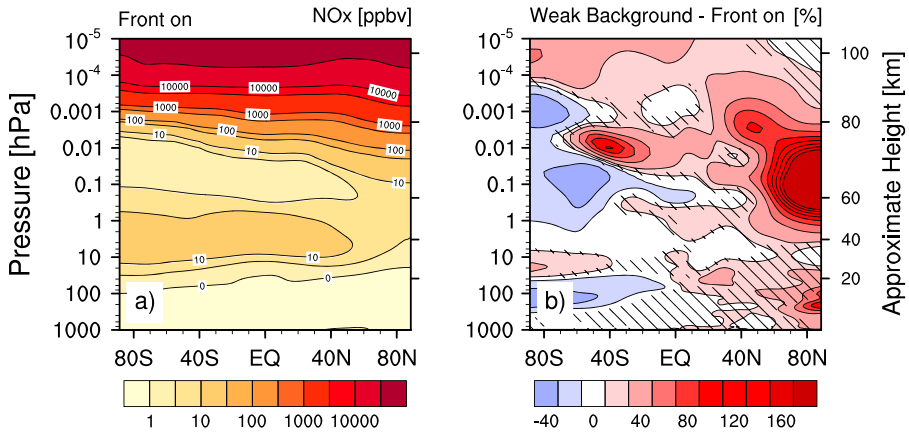

Figure 9. (a) Zonal mean NO_x volume mixing ratio averaged over December–February (DJF) for the free-running simulation front on. (b) Difference in zonal mean NO_x volume mixing ratio (DJF) between two free-running simulations (weak background-front on). Shaded areas are not significant at the 95% confidence interval. The mean over 49 years is used.

HAMMONIA is general too cold (warm). However, the changes induced by weakening the background source bring the mesopause in HAMMONIA closer to the observations.

4. Summary and Conclusion

In this study, we analyzed the impact of parameterized nonorographic gravity wave sources on the simulated transport of nitrogen oxides (NO_x) in the polar winter mesosphere. Simulations with the general circulation and chemistry model HAMMONIA were carried out in both nudged and free-running simulations mode. We analyzed differences in a homogeneous background source and in a source related to frontal activity.

Recent studies showed that parameterized nonorographic gravity waves drive the middle atmospheric dynamics after a sudden stratospheric warming (SSW) event (e.g., the descent of the elevated stratopause, the downward transport of tracers) [*McLandress et al.*, 2013; *Ren et al.*, 2011; *Siskind et al.*, 2010]. Following their analysis we found that the transport of NO_x is highly sensitive to differences in nonorographic gravity waves. Compared to a control simulation, we either strengthen the gravity wave sources (i.e., an increase of the wave amplitude) by switching on the emission of gravity waves from fronts or by increasing the background source or weaken the background source. Strengthening the gravity wave sources (frontal or background source) reduces the transport of NO_x to the mesosphere after the SSW and leads to a quicker descent of the elevated stratopause to its climatological altitude. If we weaken the background source, the transport of NO_x after the SSW is enhanced and the elevated stratopause stays longer at a higher altitude. This result may seem counterintuitive as gravity waves are considered as the key driver of downwelling in the winter mesosphere. One might assume that more wave activity would strengthen the downwelling and, hence, the tracer transport. However, in our experiments the amount of NO_x transported downward is controlled by the altitude of the largest gravity wave drag and hence by the vertical extent of downwelling. In the upper mesosphere and lower thermosphere resolved waves strongly contribute to the strengthening of the vertical wind. In other words, resolved waves amplify the enhanced downwelling originally caused by gravity waves. With weaker gravity waves the maximum in the gravity wave drag is shifted upward leading to the strongest transport in all of our simulations. This results from the smallest total variance at launching level used in all simulations, because the level at which the wave amplitude becomes unstable is then highest. Our findings extend the diagnosis of the sensitivity of the circulation to the breaking height to the upper mesosphere, as discussed in the context of the gravity waves from fronts by *Charron and Manzini* [2002]. Our results agree with *McLandress et al.* [2013], who showed that the downwelling under undisturbed conditions in an experiment with only nonorographic gravity waves (i.e., with weak gravity wave sources) is 2 times stronger than in a control run.

In line with *Siskind et al.* [2015] we show that simulations with a free-running mesosphere have among others deficits in simulating a realistic gravity wave drag in the upper mesosphere. They suggested that a weak mesospheric transport is produced by an underestimated nonorographic gravity wave drag. However, our main result is that not only the magnitude of the drag but also its altitude distribution are key to transporting NO_x downward. Both parameters can be manipulated via tuning the gravity wave sources. We have shown that a reduction of the gravity wave amplitude at source level leads to an increased momentum deposition in the upper mesosphere and, hence, to an increased (and in our case a fairly realistic) downward transport of NO_x.

We now briefly discuss the implications of our study. First, for the proper estimation of the indirect effect of energetic particle precipitation, i.e., circulation effects of NO_x produced in the lower thermosphere and transported downward during polar night, a realistic simulation of this transport is necessary in addition to a realistic representation of energetic particle sources. The underestimation of the transport in earlier modeling studies may be reduced through a reduction of parameterized gravity wave sources.

Second, due to the high uncertainty in observed momentum flux, the gravity wave parameterization cannot be constrained by direct observations. The need to adjust parameters in the models may provide the opportunity for an indirect constraint of gravity wave sources. *McLandress et al.* [2013] have suggested simulations of the downward transport for this purpose, as used here. Our simulations suggest that the magnitude of gravity wave sources may be less than assumed in earlier simulations. However, we cannot exclude that the vertical shift of the gravity wave maximum which influences strongly the downward transport of NO_x may be reached by other ways of tuning the parameterization, e.g., the launching level or cutoff wave number. In a similar sense, parameters of the frontal gravity wave source may be tuned, which may lead to a higher momentum deposition in the mesosphere. We are not implying that more realistic gravity wave parameterizations (e.g., including effects from fronts) lead to less realistic simulations of mesospheric transport in general.

It is possible that in our case, the exclusion of specific frontal sources leads to an improvement via compensation of errors. More complex gravity wave parameterization (e.g., considering lateral propagation of waves) may have a different impact on the simulated transport. Improved attempts to observe gravity waves from satellite as suggested by *Geller et al.* [2013] seem still key for a better quantification and a more realistic parameterization of their effects.

Finally, this study concentrated on the northern polar winter, but changing gravity waves affects, of course, also other regions (e.g., Tropics or Southern Hemisphere). In our first set of simulations, the dynamics of the troposphere and stratosphere were prevented to strongly drift apart by the nudging. Free-running simulations show a substantial change in the zonal wind due to differences in gravity wave sources. For an experiment with a weak background and no frontal source, the stratospheric zonal wind extends in both hemispheres further to the pole, which is consistent with MERRA reanalysis data. Furthermore, higher NO_x concentrations in the polar mesosphere for this experiment agree with the results of the nudged simulations. Hence, nudged and free-running simulations highlight the importance of momentum deposition in the upper mesosphere for a realistic NO_x transport.

Acknowledgments
The authors acknowledge scientific and practical input from Ulrike Niemeier and Manuel López-Puertas. This study was supported by the Max-Planck-Gesellschaft (MPG), and computational resources were made available by Deutsches Klimarechenzentrum (DKRZ) through support from Bundesministerium für Bildung und Forschung (BMBF). The IAA team was supported by the Spanish MCINN under grant ESP2014-54362-P and EC FEDER funds. Katharina Meraner acknowledges support from COST ActionES1005. The work has benefited from discussions within the ISSI team on coupling stratospheric warming led by Nick Pedatella. The authors thank the anonymous referees for useful comments and suggestions. The MERRA data are available through http://disc.sci.gsfc.nasa.gov/daac-bin/DataHoldings.pl. Primary data and scripts used in the analysis and other supporting information that may be useful in reproducing this work are archived by the Max Planck Institute for Meteorology and can be obtained by contacting publications@mpimet.mpg.de.

References

Alexander, M. J. (2015), Global and seasonal variations in three-dimensional gravity wave momentum flux from satellite limb-sounding temperatures, *Geophys. Res. Lett.*, *42*, 6860–6867, doi:10.1002/2015GL065234.

Alexander, M. J., et al. (2010), Recent developments in gravity-wave effects in climate models and the global distribution of gravity-wave momentum flux from observations and models, *Q. J. R. Meteorol. Soc.*, *136*(650), 1103–1124, doi:10.1002/qj.637.

Baumgaertner, A. J. G., A. Seppälä, P. Jöckel, and M. A. Clilverd (2011), Geomagnetic activity related NO_x enhancements and polar surface air temperature variability in a chemistry climate model: Modulation of the NAM index, *Atmos. Chem. Phys.*, *11*(9), 4521–4531, doi:10.5194/acp-11-4521-2011.

Bender, S., M. Sinnhuber, T. von Clarmann, G. Stiller, B. Funke, M. López-Puertas, J. Urban, K. Pérot, K. A. Walker, and J. P. Burrows (2015), Comparison of nitric oxide measurements in the mesosphere and lower thermosphere from ACE-FTS, MIPAS, SCIAMACHY, and SMR, *Atmos. Meas. Tech.*, *8*(10), 4171–4195, doi:10.5194/amt-8-4171-2015.

Chandran, A., R. R. Garcia, R. L. Collins, and L. C. Chang (2013), Secondary planetary waves in the middle and upper atmosphere following the stratospheric sudden warming event of January 2012, *Geophys. Res. Lett.*, *40*, 1861–1867, doi:10.1002/grl.50373.

Charron, M., and E. Manzini (2002), Gravity waves from fronts: Parameterization and middle atmosphere response in a general circulation model, *J. Atmos. Sci.*, *59*(5), 923–941, doi:10.1175/1520-0469(2002)059<0923:GWFFPA>2.0.CO;2.

Dee, D. P., et al. (2011), The ERA-Interim reanalysis: Configuration and performance of the data assimilation system, *Q. J. R. Meteorol. Soc.*, *137*(656), 553–597, doi:10.1002/qj.828.

Fischer, H., et al. (2008), MIPAS: An instrument for atmospheric and climate research, *Atmos. Chem. Phys.*, *8*(8), 2151–2188, doi:10.5194/acp-8-2151-2008.

Funke, B., M. López-Puertas, S. Gil-López, T. von Clarmann, G. P. Stiller, H. Fischer, and S. Kellmann (2005), Downward transport of upper atmospheric NO_x into the polar stratosphere and lower mesosphere during the Antarctic 2003 and Arctic 2002/2003 winters, *J. Geophys. Res.*, *110*, D24308, doi:10.1029/2005JD006463.

Funke, B., et al. (2011), Composition changes after the "Halloween" solar proton event: The high energy particle precipitation in the atmosphere (HEPPA) model versus MIPAS data intercomparison study, *Atmos. Chem. Phys.*, *11*(17), 9089–9139, doi:10.5194/acp-11-9089-2011.

García-Comas, M., et al. (2014), MIPAS temperature from the stratosphere to the lower thermosphere: Comparison of vM21 with ACE-FTS, MLS, OSIRIS, SABER, SOFIE and lidar measurements, *Atmos. Meas. Tech.*, *7*(11), 3633–3651, doi:10.5194/amt-7-3633-2014.

Geller, M. A., et al. (2013), A comparison between gravity wave momentum fluxes in observations and climate models, *J. Clim.*, *26*(17), 6383–6405, doi:10.1175/JCLI-D-12-00545.1.

Haynes, P. H., M. E. McIntyre, T. G. Shepherd, C. J. Marks, and K. P. Shine (1991), On the downward control of extratropical diabatic circulations by eddy-induced mean zonal forces, *J. Atmos. Sci.*, *48*(4), 651–678, doi:10.1175/1520-0469(1991)048<0651:OTCOED>2.0.CO;2.

Hines, C. O. (1997a), Doppler-spread parameterization of gravity-wave momentum deposition in the middle atmosphere. Part 1: Basic formulation, *J. Atmos. Sol. Terr. Phys.*, *59*(4), 371–386, doi:10.1016/S1364-6826(96)00079-X.

Hines, C. O. (1997b), Doppler-spread parameterization of gravity-wave momentum deposition in the middle atmosphere. Part 2: Broad and quasi monochromatic spectra, and implementation, *J. Atmos. Sol. Terr. Phys.*, *59*(4), 387–400, doi:10.1016/S1364-6826(96)00080-6.

Holt, L. A., C. E. Randall, E. D. Peck, D. R. Marsh, A. K. Smith, and V. L. Harvey (2013), The influence of major sudden stratospheric warming and elevated stratopause events on the effects of energetic particle precipitation in WACCM, *J. Geophys. Res. Atmos.*, *118*, 11,636–11,646, doi:10.1002/2013JD020294.

Holton, J. R., P. H. Haynes, M. E. McIntyre, A. R. Douglass, R. B. Rood, and L. Pfister (1995), Stratosphere-troposphere exchange, *Rev. Geophys.*, *33*(4), 403–439, doi:10.1029/95RG02097.

Kieser, J. (2011), *The Influence of Precipitating Solar and Magnetospheric Energetic Charged Particles on the Entire Atmosphere Simulations with HAMMONIA*, Max-Planck-Inst. für Meteorologie, Germany.

Kinnison, D. E., et al. (2007), Sensitivity of chemical tracers to meteorological parameters in the MOZART-3 chemical transport model, *J. Geophys. Res.*, *112*, D20302, doi:10.1029/2006JD007879.

Limpasuvan, V., J. H. Richter, Y. J. Orsolini, F. Stordal, and O.-K. Kvissel (2012), The roles of planetary and gravity waves during a major stratospheric sudden warming as characterized in WACCM, *J. Atmos. Sol. Terr. Phys.*, *78–79*, 84–98, doi:10.1016/j.jastp.2011.03.004.

Limpasuvan, V., Y. J. Orsolini, A. Chandran, R. R. Garcia, and A. K. Smith (2016), On the composite response of the MLT to major sudden stratospheric warming events with elevated stratopause, *J. Geophys. Res. Atmos.*, *121*, 4518–4537, doi:10.1002/2015JD024401.

Lott, F., and M. J. Miller (1997), A new subgrid-scale orographic drag parametrization: Its formulation and testing, *Q. J. R. Meteorol. Soc.*, *123*(537), 101–127, doi:10.1002/qj.49712353704.

Lübken, F.-J., and U. von Zahn (1991), Thermal structure of the mesopause region at polar latitudes, *J. Geophys. Res.*, *96*(D11), 20,841–20,857, doi:10.1029/91JD02018.

Manney, G. L., M. J. Schwartz, K. Krüger, M. L. Santee, S. Pawson, J. N. Lee, W. H. Daffer, R. A. Fuller, and N. J. Livesey (2009), Aura Microwave Limb Sounder observations of dynamics and transport during the record-breaking 2009 Arctic stratospheric major warming, *Geophys. Res. Lett.*, *36*, L12815, doi:10.1029/2009GL038586.

Manzini, E., and N. A. McFarlane (1998), The effect of varying the source spectrum of a gravity wave parameterization in a middle atmosphere general circulation model, *J. Geophys. Res.*, *103*(D24), 31,523–31,539, doi:10.1029/98JD02274.

McLandress, C., J. F. Scinocca, T. G. Shepherd, M. C. Reader, and G. L. Manney (2013), Dynamical control of the mesosphere by orographic and nonorographic gravity wave drag during the extended northern winters of 2006 and 2009, *J. Atmos. Sci.*, *70*(7), 2152–2169, doi:10.1175/JAS-D-12-0297.1.

Meraner, K., and H. Schmidt (2016), Transport of nitrogen oxides through the winter mesopause in HAMMONIA, *J. Geophys. Res. Atmos.*, *121*, 2556–2570, doi:10.1002/2015JD024136.

Pedatella, N. M., et al. (2014), The neutral dynamics during the 2009 sudden stratosphere warming simulated by different whole atmosphere models, *J. Geophys. Res. Space Physics*, *119*, 1306–1324, doi:10.1002/2013JA019421.

Randall, C. E., V. L. Harvey, C. S. Singleton, S. M. Bailey, P. F. Bernath, M. Codrescu, H. Nakajima, and J. M. Russell (2007), Energetic particle precipitation effects on the Southern Hemisphere stratosphere in 1992–2005, *J. Geophys. Res.*, *112*, D08308, doi:10.1029/2006JD007696.

Randall, C. E., V. L. Harvey, D. E. Siskind, J. France, P. F. Bernath, C. D. Boone, and K. A. Walker (2009), NO_x descent in the arctic middle atmosphere in early 2009, *Geophys. Res. Lett.*, *36*, L18811, doi:10.1029/2009GL039706.

Ren, S., S. Polavarapu, S. R. Beagley, Y. Nezlin, and Y. J. Rochon (2011), The impact of gravity wave drag on mesospheric analyses of the 2006 stratospheric major warming, *J. Geophys. Res.*, *116*, D19116, doi:10.1029/2011JD015943.

Richter, J. H., F. Sassi, and R. R. Garcia (2010), Toward a physically based gravity wave source parameterization in a general circulation model, *J. Atmos. Sci.*, *67*(1), 136–156, doi:10.1175/2009JAS3112.1.

Rienecker, M. M., et al. (2011), MERRA: NASA's modern-era retrospective analysis for research and applications, *J. Clim.*, *24*(14), 3624–3648, doi:10.1175/JCLI-D-11-00015.1.

Roeckner, E., R. Brokopf, M. Esch, M. Giorgetta, S. Hagemann, L. Kornblueh, E. Manzini, U. Schlese, and U. Schulzweida (2006), Sensitivity of simulated climate to horizontal and vertical resolution in the ECHAM5 atmosphere model, *J. Clim.*, *19*(16), 3771–3791, doi:10.1175/JCLI3824.1.

Rozanov, E., L. Callis, M. Schlesinger, F. Yang, N. Andronova, and V. Zubov (2005), Atmospheric response to NO_y source due to energetic electron precipitation, *Geophys. Res. Lett.*, *32*, L14811, doi:10.1029/2005GL023041.

Salmi, S.-M., P. T. Verronen, L. Thölix, E. Kyrölä, L. Backman, A. Y. Karpechko, and A. Seppälä (2011), Mesosphere-to-stratosphere descent of odd nitrogen in February–March 2009 after sudden stratospheric warming, *Atmos. Chem. Phys.*, *11*(10), 4645–4655, doi:10.5194/acp-11-4645-2011.

Scaife, A. A., N. Butchart, C. D. Warner, D. Stainforth, W. Norton, and J. Austin (2000), Realistic quasi-biennial oscillations in a simulation of the global climate, *Geophys. Res. Lett.*, *27*(21), 3481–3484, doi:10.1029/2000GL011625.

Schmidt, H., G. P. Brasseur, M. Charron, E. Manzini, M. A. Giorgetta, T. Diehl, V. I. Fomichev, D. Kinnison, D. Marsh, and S. Walters (2006), The HAMMONIA chemistry climate model: Sensitivity of the mesopause region to the 11-year solar cycle and CO_2 doubling, *J. Clim.*, *19*(16), 3903–3931, doi:10.1175/JCLI3829.1.

Seppälä, A., C. E. Randall, M. A. Clilverd, E. Rozanov, and C. J. Rodger (2009), Geomagnetic activity and polar surface air temperature variability, *J. Geophys. Res.*, *114*, A10312, doi:10.1029/2008JA014029.

Sigmond, M., and T. G. Shepherd (2014), Compensation between resolved wave driving and parameterized orographic gravity wave driving of the Brewer–Dobson circulation and its response to climate change, *J. Clim.*, *27*(14), 5601–5610, doi:10.1175/JCLI-D-13-00644.1.

Siskind, D. E., L. Coy, and P. Espy (2005), Observations of stratospheric warmings and mesospheric coolings by the TIMED SABER instrument, *Geophys. Res. Lett.*, *32*, L09804, doi:10.1029/2005GL022399.

Siskind, D. E., S. D. Eckermann, L. Coy, J. P. McCormack, and C. E. Randall (2007), On recent interannual variability of the arctic winter mesosphere: Implications for tracer descent, *Geophys. Res. Lett.*, *34*, L09806, doi:10.1029/2007GL029293.

Siskind, D. E., S. D. Eckermann, J. P. McCormack, L. Coy, K. W. Hoppel, and N. L. Baker (2010), Case studies of the mesospheric response to recent minor, major, and extended stratospheric warmings, *J. Geophys. Res.*, *115*, D00N03, doi:10.1029/2010JD014114.

Siskind, D. E., F. Sassi, C. E. Randall, V. L. Harvey, M. E. Hervig, and S. M. Bailey (2015), Is a high-altitude meteorological analysis necessary to simulate thermosphere-stratosphere coupling?*Geophys. Res. Lett.*, *42*, 8225–8230, doi:10.1002/2015GL065838.

Smith, A. K., R. R. Garcia, D. R. Marsh, and J. H. Richter (2011), WACCM simulations of the mean circulation and trace species transport in the winter mesosphere, *J. Geophys. Res.*, *116*, D20115, doi:10.1029/2011JD016083.

Tomikawa, Y., K. Sato, S. Watanabe, Y. Kawatani, K. Miyazaki, and M. Takahashi (2012), Growth of planetary waves and the formation of an elevated stratopause after a major stratospheric sudden warming in a T213l256 GCM, *J. Geophys. Res.*, *117*, D16101, doi:10.1029/2011JD017243.

Wissing, J. M., and M.-B. Kallenrode (2009), Atmospheric ionization module Osnabrück (AIMOS): A 3-D model to determine atmospheric ionization by energetic charged particles from different populations, *J. Geophys. Res.*, *114*, A06104, doi:10.1029/2008JA013884.